DEPARTAMENTO DE MATEMÁTICA
DOCUMENTO DE TRABAJO

"Analysis of puff dynamics in oocytes: interdependence of puff amplitude and inter-puff interval"

Daniel Fraiman, Bernardo Pando, Sheila Dargan,
Ian Parker y Silvina Ponce Dawson

D.T.: N° 33 Abril 2005

Vito Dumas 284, (B1644BID) Victoria, Pcia. de Buenos Aires, Argentina
Tel: 4725-7053 Fax: 4725-7010
Email: matematica@udesa.edu.ar

Analysis of puff dynamics in oocytes: interdependence of puff amplitude and inter-puff interval

Daniel Fraiman[1], Bernardo Pando[1], Sheila Dargan[2], Ian Parker[2], Silvina Ponce Dawson[1]
[1] Departamento de Física, Facultad de Ciencias Exactas y Naturales, U.B.A., Ciudad Universitaria, Pabellón I (1428) Buenos Aires, Argentina.
[2] Department of Neurobiology and Behavior, University of California, Irvine, CA 92697-4561, U.S.A.

ABSTRACT

Puffs are localized Ca^{2+} signals that arise in oocytes in response to inositol 1,4,5-trisphosphate (IP_3). They are analogous to the sparks of myocytes and are believed to be the result of the liberation of Ca^{2+} from the endoplasmic reticulum through the coordinated opening of IP_3-receptor/channels clustered at a functional release site. In this paper we analyze sequences of puffs that occur at the same site to help elucidate the mechanisms underlying puff dynamics. In particular, we show a dependence of the inter-puff time on the amplitude of the preceding puff, and of the amplitude of the following puff on the preceding interval. These relationships can be accounted for by an inhibitory role of the Ca^{2+} that is liberated during puffs. We construct a stochastic model for a cluster of IP_3-receptor/ channels that quantitatively replicates the observed behavior, and determine that the characteristic time for a channel to escape from the inhibitory state is of the order of seconds.

INTRODUCTION

The inositol 1,4,5-trisphosphate (IP_3) receptor (IP_3R) is a ligand-gated intracellular Ca^{2+} release channel that plays a central role in modulating cytoplasmic Ca^{2+} concentration and provides a link between cell surface receptors and Ca^{2+} release from intracellular stores. In addition to their regulation by IP_3, IP_3R´s show a biphasic modulation by cytosolic Ca^{2+}; for relatively low [Ca^{2+}] the channel open probability increases with [Ca^{2+}], whereas it reduces at high [Ca^{2+}] (1,2,3,4,5).

The spatio-temporal properties of signals arising through IP_3R's have been extensively characterized by optical imaging in *Xenopus laevis* oocytes (6). These studies have revealed a hierarchical organization of release events, ranging from [Ca^{2+}] liberation from single IP_3R's ("blips"), through the concerted opening of several IP_3R's within a cluster ("puffs") to global waves involving cluster-cluster interactions via [Ca^{2+}]-induced [Ca^{2+}] liberation (7). Puffs have also been observed in many other cell types (8,9,10,11), and appear to represent ubiquitous "elementary events" of intracellular [Ca^{2+}] signaling, which can both have local signaling functions in their own right, and serve as building blocks from which global signals are constructed.

It is, therefore, important to understand the mechanisms underlying the generation and modulation of puffs. However, several aspects of puff dynamics still await clarification; most importantly, the mechanisms of puff termination and subsequent recovery of excitability. Given that Ca^{2+} is both a ligand of the IP_3R that affects its open probability and is the main ion carrier that flows through its pore, the Ca^{2+} ions that are released in the cytosol during a puff are expected to modulate the dynamics of a puff. Ca^{2+} release through a single IP_3R in a cluster may thus induce the regenerative opening of neighboring channels, which subsequently close because of the inhibitory effect of high local Ca^{2+} levels attained during the puff. Additional processes, however may also affect puff termination; including the local depletion of luminal Ca^{2+} (an effect that is present in the case of sparks (12,13)), or the effect of counter-ions (14).

In this paper we examine the effects of cytosolic Ca^{2+} on puff dynamics by investigating the distributions of intervals between successive puffs occurring at a given site. Experimental data were obtained by fluorescence imaging of puffs evoked in *Xenopus laevis* oocytes by continuous photorelease of IP_3, and were analyzed to look for correlations between puff amplitudes and inter-puff intervals. We find strong dependences between puff size and inter-puff interval which can be explained in terms of an inhibitory role of Ca^{2+} binding to a cytosolic site on the IP_3R. Furthermore, by analyzing a simple model that reproduces the observed distributions we determine that the characteristic time for Ca^{2+} binding to this site is of the order of seconds.

MATERIALS AND METHODS

Experimental procedure

Preparation of Xenopus oocytes

Xenopus laevis were anesthetized by immersion in 0.17% MS-222 for 15 min and sacrificed by decapitation in adherence with protocols approved by the UC Irvine Institutional Animal Care and Use Committee. Oocytes (stage V - VI) were manually plucked and collagenase-treated (0.5mg.ml^{-1} for 30 min) before storage in Barth's solution (composition in mM: NaCl, 88; KCl, 1; $NaHCO_3$, 2.4; $MgSO_4$, 0.82; $Ca(NO_3)_2$, 0.33; $CaCl_2$, 0.41; HEPES, 5; pH 7.4) containing 0.1mg.ml^{-1} gentamicin at 17 ^{o}C for 1–7 days before use. Intracellular microinjections were performed using a Drummond microinjector to load oocytes with Oregon Green 488 BAPTA 1 (OG-1) together with caged IP_3 (D-myo-inositol 1,4,5-trisphosphate, $P_{4(5)}$-(1-(2-nitrophenyl)ethyl) ester) and EGTA to respective final intracellular concentrations of 40, 4, and 270μM; assuming 1 μl cytosolic volume.

Confocal laser scanning microscopy

Confocal Ca^{2+} images were obtained using a custom-built line-scan confocal scanner interfaced to an Olympus IX70 inverted microscope (15). Recordings were made at room temperature, imaging in the animal hemisphere of oocytes bathed in normal Ringer's solution (composition in mM: $NaCl_2$, 120; KCl, 2; $CaCl_2$, 1.8; HEPES, 5; pH 7.3). The laser spot of a 488 nm Argon ion laser was focused with a 40X oil immersion objective (NA 1.35) and scanned every 8 ms along a 100 μm line. Emitted fluorescence was detected at wavelengths > 510nm through a confocal pinhole providing lateral and axial resolutions of about 0.3 and 0.5μm, respectively. The scan line was focused at the level of the pigment granules and images were collected through a cover glass forming the base of the recording chamber. IP_3 was photo-released from a caged precursor by delivering UV light, focused uniformly throughout a 200 μm spot surrounding the image scan line. After imaging resting fluorescence for 2s, the UV light was turned on continually throughout the remainder of the record (1 min), with the rate of photorelease of IP_3 controlled by a continuously variable neutral density filter.

Data processing and pooling

Fig. 1 A shows a typical experimental record in which fluorescence ratio changes, $\Delta F(x,t)/F_0$, are depicted using a color-code on a time-space plot (t,x). Here $\Delta F(x,t) \equiv F(x,t)-F_0$ and $F_0 \equiv \langle F(x,t<0)\rangle_t$, where the average is performed at each spatial point, *x*, over a certain number (ca. 50) of times prior to IP_3 photorelease. The relative fluorescence is used in order to compensate for local inhomogeneities of the oocyte or of the dye distribution (16). EGTA was added to the injection solution (270 μM final cytosolic concentration) to functionally uncouple Ca^{2+} release sites, resulting in discrete puffs without propagating Ca^{2+} waves (17). For example, the linescan image in Fig. 1 A illustrates puffs generated at numerous sites, and Fig. 1 B shows the corresponding fluorescence ratios measured at five sites. The

fluorescence ratio is directly related to the amount of Ca^{2+} -bound dye, [CaD] (16), but owing to the restricted time and space resolution of the imaging system such records can only provide information on the average concentration over a finite volume. When the dye is not saturated (which is the case in these experiments: $\Delta F(x,t)/F_0 <<$ maximal change of ~10 in saturating [Ca^{2+}]) the spatio-temporal distribution of [CaD] should correspond about linearly to free Ca^{2+}.

Analyses were done on fluorescence profiles like those in Fig. 1 B from 46 different puff sites. We computed the local temporal average and the standard deviation of the fluorescence signal at a site using windows of the order of 2s (*i.e.*, of the order of the inter-puff time and much longer than a typical puff duration) and identified the onset of a puff when the instantaneous fluorescence ratio exceeded the average value of the corresponding window by 3 standard deviations. The amplitude of the event, *A*, was taken as the maximum fluorescence ratio ($\Delta F(x,t)/F_0$) during the puff.

Ideally, we would like to work with very long records showing many release events at the same site. However, that was impracticable because of movement artifacts and eventual rundown of puffs. Instead, we grouped data from different release sites; typically with around 13 events observed at a given site. Because of the wide variation in puff amplitudes between different sites (possibly reflecting differences in numbers of channels per cluster) we classified release sites according to the size of the largest event observed at each. Fig. 2 shows the maximum puff amplitudes recorded from each of the 46 sites analyzed. We arbitrarily defined two groups of "small" (filled circles) and "large" clusters (crosses); representing a compromise between size of the resultant data sets and "homogeneity" of the clusters properties. All analyses presented here were based on events from the small cluster group (18 release sites and 232 puffs). Similar results regarding the dependence between puff amplitude and inter-puff times were obtained when the analysis was restricted to the group of large clusters (see Table 1).

Statistical tests and parameter fitting

Results are presented as frequency histograms of occurrence of certain subsets of events (*e.g.*, puffs with amplitude within a certain range, etc). The corresponding distribution of frequencies of the variable of interest (*e.g.*, amplitude or inter-puff time), $P_n(x)$, was used to compute the (cumulative) empirical distribution function, $F(X)=\int_{-\infty}^{X} dx P_n(x)$. In order to compare two stochastic processes, we compare the distribution functions of some of the stochastic variables that characterize the processes. In the case of the experiments, it is the empirical distribution function that is obtained from the variable of interest. In the case of the model we analyze in this paper, we compute it as in the experimental case, using the results that come from extensive numerical simulations of the stochasic process. Once we have two distribution functions that we wish to compare, F_1 and F_2 , we compute the Kolmogorov statistics,

$$T \equiv \sup_x | F_1(x) - F_2(x) | \qquad (1)$$

Statistical significance (p-values) of differences between distributions was determined from lookup tables (18).

In this paper we present a stochastic model that reproduces the experimental observations. To determine parameter values for the model, we initially divided the parameter space with a relatively coarse grid, performed stochastic simulations for each set of parameter values in the grid and computed the cumulative distribution function, F_{sim} , for the inter-puff time. This was compared with the experimentally determined one, F_{exp} , and the initial parameter values

were rejected if a Kolomogorov test determined that the simulated and experimental values were different (p-value<0.05). Once we attained a subset of parameter values for which F_{sim} and F_{exp} were not significantly different, we refined the grid of parameter values and iteratively repeated this procedure.

RESULTS

Analysis of experimental data

Fig.3 shows histograms of puff amplitude, A, and inter-puff time, τ, for the set of events analyzed in this paper (*i.e.*, the set of small events defined in Fig. 2). The amplitude distribution is asymmetric and has a maximum around 0.1 with standard deviation, σ=0.032. The inter-puff time distribution resembles a log-normal or Gamma distribution and has a maximum around 1.5s with standard deviation, σ=1.37s. This distribution is similar to the one obtained in (6) using pooled data from three puff sites.

We analyze now the existence of dependencies between puff amplitude and inter-puff time. A scatter plot of the amplitude of the n-th event, A_n *vs*. the time elapsed from the preceding event at the same site, $\tau_{n-1} \equiv t_n - t_{n-1}$ (with t_n the time at which the n-th event occurs), did not reveal any structure (data not shown). However, various conditional distributions do display differences, reflecting the existence of dependences between puff amplitude and inter-puff time. We show in Fig. 4 the distributions of event amplitudes, A_n, grouped according to whether the elapsed time from the previous event at the same site, τ_{n-1}, was smaller than the first quantile, q_1, of the inter-puff time distribution ($\tau_{n-1}<q_1$=1.4s: panel A) or was larger than the third quantile, q_3 ($\tau_{n-1}>q_3$=3.27s: panel B). The conditional distributions are different: for "small" τ_{n-1} the next puff, on average, has a smaller amplitude than for "large" values of τ_{n-1} .

Fig. 5 shows the corresponding distributions of inter-puff times, $\tau_n = t_{n+1} - t_n$, conditional on whether the amplitude of the preceding puff, A_n, was "small" ($A_n < q_1$=0.092) or "large" ($A_n > q_3$=0.134). We again observe differences in both distributions: for small, A_n, the distribution of intervals following those puffs clusters around τ_n ~1s, whereas for large, A_n the distribution peaks near τ_n~3s and has a larger dispersion.

To further explore the relationships between puff amplitude and inter-puff time, we computed the corresponding conditional distribution functions, using two different definitions of "large" and "small" previous inter-puff time, τ_{n-1} or amplitude, A_n. Namely, we first included in the sets of small or large inter-puff times, τ_{n-1}, only the 17% with the smallest values and the 17% with the largest values, respectively. We show the distribution functions of subsequent amplitudes, A_n, obtained in this way in Fig. 6 A (curve 1 for the set of small previous inter-puff times, τ_{n-1}, and curve 4 for the set of large previous inter-puff times). The total number of events is 40 for each set in this case. We then divided the total set of previous inter-puff times in two halves: 50% of the data (116 events) in each set. We show the corresponding distribution functions of subsequent amplitudes in Fig. 6 A (curve 2 for the new set of small previous inter-puff times and curve 3 for the new set of large previous inter-puff times). A similar analysis was done for the cumulative distribution function of inter-puff times, τ_n (Fig. 6 B). These data show that the amplitude (inter-puff time) distributions conditioned to large or small previous inter-puff times (amplitudes) are different, and that the differences are more pronounced as the maximum inter-puff time (amplitude) value in the set of small times (amplitudes) becomes more different from the minimum inter-puff time (amplitude) value in the set of large values.

Table 1 summarizes the dependencies between puff amplitude and inter-puff times obtained for the group of large clusters (crosses in Fig.2). In this case, the equal distribution hypothesis is always rejected.

	A_n / τ_{n-1}	τ_n / A_n
17%	T=0.511, p-value<0.001	T=0.316,p-value=0.023
25%	T=0.437, p-value<0.001	T=0.303, p-value=0.004
50%	T=0.274, p-value<0.001	T=0.237, p-value=0.002

Table 1. Kolmogorov test for the conditional distributions of the group of "large" clusters (crosses in Fig. 2).

Mechanisms underlying correlated puff behavior

The results of Figs. 3 and 4 reveal an inhibitory effect following a puff. Namely, inter-puff intervals tend to be longer following large puffs; and puffs tend to be smaller following short intervals. Several possible mechanisms may underlie these correlations. One is that the high cytosolic [Ca^{2+}] attained during a puff inhibits channels within the cluster, so that the amplitude and probability of occurrence of a subsequent puff recover with a time course reflecting the recovery of channels from an inhibited state. Other processes that might affect the inter-puff time include local depletion of Ca^{2+} in the ER lumen leading to decreased single channel current (19) and/or affect the channel open probability (20); or the effect of counter-ions that might affect Ca^{2+} dynamics on both the cytosolic and luminal sides (14,21). Under our experimental conditions we expect local luminal [Ca^{2+}] depletion to be small (see *e.g.* (17,19,22)). In this paper we therefore explore whether the observed behavior can be accounted for by an inhibitory effect of the cytosolic [Ca^{2+}] on the channels within a cluster.

An idealized model in terms of individual channels

We developed an idealized cluster model containing a finite number of channels, N, with IP_3 bound. Given that most of the time IP_3 is bound to its corresponding site, even for relatively low values of [IP_3] (see Discussion), for simplicity, we neglect fluctuations in N due to IP_3 binding and unbinding. That would only introduce some statistical noise. Each of these N channels can exist in two main states: inhibited or uninhibited. Unihibited channels may be open (during a release event) or closed (during the inter-puff time). Since we are interested in understanding the inter-puff time distribution, not the kinetics of the puffs themselves, we assume that a release event (i.e. channel open time) is instantaneous. If a channel is in the inhibited state it has to wait a time that is exponentially distributed with mean value $1/\lambda_2$ to become unihibited. An inhibited channel cannot open. An unhibited channel opens with probability per unit time, λ_1, if all the other channels of the cluster are closed and opens with probability one if any other channel in the cluster opens; i.e. if one channel opens, calcium-induced calcium release (CICR) causes all the uninhibited channels of the cluster to open simultaneously. Several assumptions are implicit in this model. First, a sudden increase in the local cytosolic [Ca^{2+}] induces channel opening of IP_3R's with IP_3 bound before it can induce inhibition, in agreement with experimental data showing faster binding to activating site(s) on IP_3R's than to inhibitory sites (see *e.g.*, (23)). Second, the amount of Ca^{2+} released during a puff is enough to open all uninhibited channels of the cluster with IP_3 bound. This appears reasonable, given that cytosolic [Ca^{2+}] averaged over the region of a cluster reaches values of the order of 10μM during a small puff (24). The probability, λ_1, on the other hand, is related to the probability that the necessary ions bind to one channel in the cluster inducing its opening. Clearly, this depends on the concentrations of agonists (IP_3 and Ca^{2+}) and although [IP_3] can be assumed to remain constant during the experiment, the cytosolic [Ca^{2+}] changes dramatically during a puff. We assume that cytosolic [Ca^{2+}] returns close to its basal level relatively soon after the puff ends (in part, due to the presence of EGTA in the experiments

we are looking at, which "balkanizes" Ca^{2+} signals(25)). Indeed, numerical simulations of how free cytosolic [Ca^{2+}] varies upon Ca^{2+} release from the ER with a current of 0.05pA show that [Ca^{2+}] averaged over a $(20nm)^3$ region around the channel's mouth drops from ~ 40μM to less than 100nM in less than 1ms following channel closure (26) (see also (19)). This time is much shorter than the typical inter-puff time. Thus, the assumption that the cytosolic [Ca^{2+}] is around the basal level ([Ca^{2+}]~50nM) in between puffs is realistic. In the model, an unhibited channel may become inhibited in a puff with a probability, p_{inh}, that depends on the number of channels that opened during the puff, N^o. The inhibition probability, p_{inh}, is a monotomically increasing function of N^o such that $p_{inh} \to 1$ as $N^o \to \infty$. To limit the number of free parameters, we consider the exponential function, $p_{inh}(N^o)=1-(1-a).\exp(-(N^o-1)b)$, where a, and b are adjusted to match the experimental data. Similar results were obtained with a sigmoidal function (data not shown). We chose p_{inh} as an increasing function of N^o to mimic the observed inhibitory effect of puffs on the channels within the cluster. Specifically, we assumed that the larger N^o, the higher [Ca^{2+}] at the cluster and, consequently, the higher the probability of channels in the cluster becoming inhibited. We show in Fig. 7 the system dynamics that apply when Ca^{2+} binding to an "activating" site is the rate limiting process for opening of uninhibited channels. This assumption holds for the IP_3R if [Ca^{2+}] is close to its basal value ([Ca^{2+}]~50nM), as we are assuming is the case in-between puffs.

We can relate the parameters, λ_1, λ_2, a and b of the model to properties of single IP_3R's. Namely, λ_1 is the probability per unit time that the necessary number of Ca^{2+} ions binds to activating sites of an IP_3R with IP_3 bound and induce channel opening. Assuming that IP_3R inhibition is only due to the inhibiting effect of cytosolic Ca^{2+}, λ_2 is then the probability per unit time at which Ca^{2+} unbinds from the inhibiting site(s). Since we find that $1/\lambda_2$ is relatively large, which means that it takes a relatively long time for the channel to become uninhibited, we can assume that the function $p_{inh}(N^o)$ is mainly determined by the stationary open probability at the (high) cytosolic [Ca^{2+}] that is achieved near the channel's mouth during a puff. Namely, we can assume that $1-p_{inh}(N^o)$ provides an upper bound of this open probability, $P_o([Ca^{2+}]) \leq 1-p_{inh}(N^o)=(1-a)\exp(-(N^o-1)b)$, so that $1-a \geq P_o([Ca^{2+}])$ and b^{-1} gives the rate at which P_o decreases with with N^o or, equivalently, with cytosolic [Ca^{2+}] at the high concentrations that are reached during the puff (see Discussion).

Estimating the model parameters from the experimental data

We adjusted the parameters of the model to minimize the value of T defined in Eq. (1) with F_1 equal to the (cumulative) distribution function of inter-puff times obtained experimentally (displayed in Fig. 3 B)) and F_2 equal to the one obtained from the model. Given that we are not using any of the conditional distributions shown in Figs. 4 and 5 to fit the parameters, the subsequent ability of the model to reproduce these conditional distributions serves as a validation of the model. This fitting procedure cannot provide the value of N. On the other hand, the values of λ_1 and λ_2 should be related to N (*e.g.*, if we decrease N, we expect the fitted values of λ_1 to get larger in order to obtain the experimentally determined mean inter-puff time). We could find N if we had a way to determine the relationship between puff amplitude, A, and number of open channels, N^o. If we assume that the smallest events that we observe correspond to $N^o=1$ and the largest ones to $N^o=N$ (for the type of cluster that we are analyzing) and that there is a linear relationship between A and N^o, then we could estimate from Fig. 4 A), that N (the number of channels with IP_3 bound) is around 4 or 5. This number coincides with the typical number of open channels in a puff estimated in (27). However, it is not completely clear that the relationship between relative fluorescence (amplitude) and

number of open channels should be linear (19). Therefore, we decided to repeat all the calculations for two values of N, N=4 and N=16.

For N=4, the best parameter values that we find are: λ_1=0.225s^{-1}, λ_2 =0.4s^{-1} , *a*=0.8, and *b*=1.8, for which the test defined by Eq. 1 gives T=0.07 (p-value=0.22, *i.e.*, the hypothesis that the two distributions are the same cannot be rejected). For N=16, the best parameter values that we find are: λ_1=0.043s^{-1}, λ_2 =0.67s^{-1}, *a*=0.6 and *b*=1.5, for which the test defined by Eq. 1 gives T=0.08 (p-value=0.11). These pararameter values are contrasted against single IP_3R properties in the Discussion section.

Model results

In order to check that the model in fact reproduces the inter-puff time distribution that was used for the fitting and to test its ability to reproduce other features of the experimentally determined distributions not enforced with the fitting, we performed numerical simulations using N=4, λ_1=0.225s^{-1}, λ_2 =0.4s^{-1} a=0.8, and b=1.8. We show in Fig. 8 the histograms of the number of open channels in a puff, N^o, and of the inter-puff times, τ, obtained with these simulations. As expected, the τ distribution thus obtained is statistically indistinguishable from the experimental one (compare Fig. 8 B) and 3 B)). The Kolmogorov statitics is T=0.07, giving a p-value=0.22 for the equal distribution null hypothesis. A quantitative comparison of the N^o distribution and the amplitude distribution histogram is not possible at this time because we do not know the relationship between puff amplitude and number of open channels.

We show in Fig. 9 the conditional distributions of the number of open channels for the sets of small (τ<1.4s) and large (τ>3.27s) previous inter-puff times. Although we do not know the relationship between observed puff amplitude and number of open channels, the way the histograms change as we condition them to small (A) or large (B) previous inter-puff times is qualitatively similar to the change observed experimentally and shown in Fig. 4.

We show in Fig. 10 the conditional distributions of inter-puff times for the set of small, $N^o \leq$ 2, and large, $N^o \geq$ 3, previous number of open channels, N^o. Also in this case, the agreement with the observations of Fig. 5 is very good. Furthermore the Kolmogorov test does not reject the equal distribution hypothesis between the simulated conditional distributions and the experimental ones (p-values>0.5).

We repeated all these computations using N=16. Also in this case, the test defined by Eq. 1 gives a reasonably good value, (p-value=0.11) for which the hypothesis that the inter-puff time distribution functions obtained with the model and with the experiments are the same cannot be rejected. However, while three of the parameter values that we obtain with the fitting procedure are similar to the N=4 case (λ_2 =0.67s^{-1}, *a*=0.6 and *b*=1.5), the value of λ_1 (λ_1=0.043s^{-1}) is harder to justify from the point of view of the single IP_3R dynamics. If we relate it to the rate of Ca^{2+} binding to n activating sites of the IP_3R in the absence of inhibition (see Discussion), using the rates of the DeYoung-Keizer model (23) we obtain n=7, which is too large. On the other hand, while the various conditional distribution functions analyzed in this paper are qualitatively similar to the experimentally determined ones, the Kolomogorov tests give p-values that are not as good as in the N=4 case (p-value=0.022 for the set of small previous amplitudes and p-value=0.094 for the set of large previous amplitudes). For this reason, all subsequent results will be restricted to the N=4 case.

Model predictions and suggested further tests

The simple model introduced in this paper explains the experimentally observed distributions of puff amplitude and inter-puff times in terms of the competition between two basic processes: inhibition and channel opening. The degree of inhibition is related to the amount of Ca^{2+} that is released during a puff and, at the single channel level, the typical timescale of inhibition is given by $1/\lambda_2$. In the model, the opening of the first channel during a puff is triggered by random binding of Ca^{2+} at basal cytosolic [Ca^{2+}] levels with a typical timescale given by $1/\lambda_1$. The fitting of the previous section gives us that $1/\lambda_1 > 1/\lambda_2$, which means that, typically, each channel becomes uninhibited faster than the rate at which it is challenged by basal Ca^{2+} to become open. Under the assumptions for which the model works, IP_3 enters mainly to determine the effective number of IP_3R's in a cluster, N, that are amenable to make a transition to the open state (and contribute to a puff). This number does affect the statistics of the cluster as a whole. It is thus of interest to analyze how the mean puff amplitude and the mean inter-puff times change when the balance between inhibition and channel opening are changed by a change in the rates at which they occur at the single channel level, or by a change in the number of "available" IP_3R's in a cluster.

In order to investigate how the various intervening factors affect puff dynamics, we performed numerical simulations keeping the same values as before for all parameters but one and investigated how the mean number of open channels at a site during a puff, $\langle N^o \rangle$, and the mean inter-puff time at the same site, $\langle \tau \rangle$, changed. We show in Figs. 11 A and 12 A the results obtained for $\lambda_1 = 0.225 s^{-1}$, $\lambda_2 = 0.4 s^{-1}$ a=0.8, b=1.8 and various values of N (N=2,3,4,5,6,7,8). N=4 corresponds to the case discussed in the previous section. We observe that $\langle \tau \rangle$ decreases and $\langle N^o \rangle$ increases when N, the number of IP_3R's in the cluster with IP_3 bound, increases. Thus, $\langle \tau \rangle$ increases with $\langle N^o \rangle$ (as N increases) as shown in Fig. 12 A. Although we do not know the exact relationship between N^o and the observed puff amplitude, A, we do expect it to be an increasing function. Therefore, based on the results of Fig. 12 A we expect the observed $\langle \tau \rangle$ to increase with $\langle A \rangle$ if this is either due to a larger amount of IP_3 or to a larger mean cluster size. In fact, if we compute the mean amplitude and inter-puff time for the set of large clusters (defined in Fig. 2) we obtain that $\langle A \rangle$ is larger and that the mean and the median inter-puff times (mean=2.48s, median=2.26s, σ=1.37s) are smaller than in the group of small clusters (mean=2.36s, median=2.04s, σ=1.37s). Although this result has the tendency predicted by Fig. 12 A, the numerical differences are not statistically significant.

We show in Figs.11 B and 12 B the dependence of mean inter-puff time, $\langle \tau \rangle$ on λ_1 for N=4, $\lambda_2 = 0.4 s^{-1}$ a=0.8, b=1.8. By increasing λ_1 we are increasing the frequency at which Ca^{2+} ions can bind to the IP_3R activating sites. Since channel opening also depends on whether the channel is inhibited or not, the net effect of increasing λ_1 will thus compete with the effect of inhibition, whose typical timescale is $1/\lambda_2$. We observe in Fig. 11 B that $\langle \tau \rangle$ decreases with λ_1, until it reaches a plateau that depends on the value of N. This is similar to the behavior of Fig. 11 A: increasing λ_1 increases the inter-puff frequency, because IP_3R's are challenged more often by the Ca^{2+} ions that are present in the cytosol in between puffs. However, the behavior of $\langle N^o \rangle$ is different in Figs. 11 A and B. Namely, $\langle N^o \rangle$ decreases with increasing λ_1 because as $1/\lambda_1$ becomes comparable with $1/\lambda_2$, the limiting process for the occurrence of a puff becomes inhibition rather than channel opening. Thus, very likely, when the first channel in a cluster opens, most of the other channels will be inhibited because not enough

time has elapsed (compared with $1/\lambda_2$). Therefore, on average, events become smaller in size than when individual IP_3R's are challenged less often (smaller λ_1). As a result, in this case, $<\tau>$ is an increasing function of $< N^o>$, as shown in Fig.12 B).

We also tested the effects of changing the probability that an uninhibited channel becomes inhibited during the occurrence of a puff, $p_{inh}(N^o)=1-(1 - a).\exp(-(N^o-1)b)$. In particular, we observed that if p_{inh} is increased, by either increasing *a* or *b*, while leaving the other parameters fixed, the mean inter-puff time, $<\tau>$ increases. The mean number of open channels during a puff, $<N^o>$, on the other hand, decreases when *b* is increased, but increases with *a* for $a<0.3$ and then, decreases (data not shown). The fact that $<\tau>$ increases with p_{inh} is very intuitive, since a larger inhibition probability should lead to a larger mean inter-puff time. As in the case of Fig. 12 B), the decreasing behavior of $<N^o>$ with p_{inh} is related to the fact that inhibition becomes the limiting process for puff occurrence as p_{inh} becomes large enough.

DISCUSSION AND CONCLUSIONS

We have analyzed sequences of "puffs" observed using optical techniques in oocytes of *Xenopus Laevis*. We have shown that there is a dependence between inter-puff time and puff amplitude for puffs that occur at the same site (cluster of channels) in the oocyte. Namely, we have determined that puffs of large amplitude are most likely followed by a long inter-puff time. Besides, puffs that occur after a large inter-puff time has elapsed are most likely large. We have shown the occurrence of this behavior in records containing relatively small puffs involving the release through very few channels (IP_3R's) that were evoked by a permanent photorelease of IP_3. Given the small amplitude of the puffs, which we expect should result in a small local Ca^{2+} depletion on the luminal side, we have investigated the possibility of explaining this behavior in terms of the inhibiting role that cytosolic Ca^{2+} can exert on IP_3R 's. To this end, we constructed a very simple stochastic model that yet retains the main features of clusters of IP_3R's. The stochastic model reproduces the observed behavior quantitatively, and provides some interesting predictions regarding the way the observed behavior would change by varying the Ca^{2+} basal concentration or $[IP_3]$.

The simple stochastic model of puff dynamics that we have introduced in this paper is characterized by three probabilities which can be related to single IP_3R properties: λ_1, the probability per unit time that an IP_3R with IP_3 bound opens at basal Ca^{2+} levels; λ_2, the probability per unit time that an (inhibited) IP_3R loses the Ca^{2+} ions that induced its inhibition; $p_{inh}(N^o)$, the probability that an IP_3R becomes inhibited during a puff.. The model is also characterized by the maximum possible number of "active" IP_3R 's in the cluster, N (*i.e.*, the number of IP_3R 's with IP_3 bound). We fixed a value of N and determined the values of the parameters that characterize the three probabilities by a fitting procedure. Most reasonable values of λ_1 and λ_2 were obtained for N=4.

Assuming that the rate of Ca^{2+} binding to one activating site is k_{on}^{act} and that Ca^{2+} binding to n (independent) activating sites is needed to induce channel opening (provided that IP_3 is already bound and that there is no Ca^{2+} bound to the inhibitory sites of the channel), then we can relate λ_1 and k_{on}^{act} by: $\lambda_1 \sim ([Ca^{2+}]/K_d)^{n-1} k_{on}^{act}[Ca^{2+}]$, where K_d is the dissociation constant of each (activating) Ca^{2+} binding site. The fitting procedure with N=4 gave $\lambda_1=0.225s^{-1}$. This value is compatible with the one that is obtained using models of the IP_3R for $[Ca^{2+}]=50nM$ and n>1. For example, if we use the DeYoung-Keizer model (28) we determine that for n=3

it is $([Ca^{2+}]/K_d)^{n-1}k_{on}^{act}[Ca^{2+}]^{+}]=0.37s^{-1}$. If we repeat this calculation using the rate, λ_1, determined with the fitting with N=16, $\lambda_1=0.043s^{-1}$, we obtain n=7, which is too large.

The value of λ_2 obtained with the fitting with N=4, $\lambda_2=0.4s^{-1}$, implies that the mean time that a channel remains inhibited is of the order of 2.5 s. If inhibition is due to Ca^{2+} binding to some cytosolic sites, $1/\lambda_2$ should provide a lower bound for the mean time that an IP_3R remains closed in single channel experiments when cytosolic $[Ca^{2+}]$ is of the order of the values that it achieves during a puff (which we estimate as ~50-120μM in a ~$(20nm)^3$ region around the channel's mouth). $1/\lambda_2=2.5s$ is much larger than the mean closed time reported in (30) for $[Ca^{2+}]=100\mu M$ and $[IP_3]=10\mu M$ with or without ATP. However, it could be compatible with the behavior at $[IP_3]=33nM$ shown in this paper (mean closed times at $[IP_3]=33nM$, are shown up to $[Ca^{2+}]=3\mu M$ only and they are of the order of 0.1s (30)). It is compatible with the values of the model presented in (31), in which the time for the recovery of IP_3R 's from Ca^{2+}-induced inactivation was estimated to be between 1.25s and 2.6s. Similar conclusions can be obtained using the value of λ_2 determined with the fitting with N=16 ($\lambda_2=0.67s^{-1}$).

Given that the time it takes for a single inactivated IP_3R to become uninhibited (~2s) is much longer than a typical puff duration (~0.05s), p_{inh} is both the probability that a single active IP_3R becomes inhibited during the time duration of a puff or the fraction of active IP_3R 's that become inhibited during a puff. Given the relatively short duration of a puff we expect p_{inh} to be smaller than the fraction of channels that are inhibited under a stationary condition of high $[Ca^{2+}]$, as the one achieved during a puff (50-120μM). In fact, it can be proven that p_{inh} is smaller than the stationary value using the rate of $[Ca^{2+}]$ binding to the inhibitory site of the DeYoung-Keizer model and the rate of inhibition release that we obtain, λ_2. The stationary probability of a channel being inhibited, on the other hand, is smaller than the stationary probability of being closed. Therefore, we can assume that $p_{inh} \leq 1- P_o([Ca^{2+}])$ with $P_o([Ca^{2+}])$ the stationary open probability at $[Ca^{2+}]$~50-120μM, from which we get that $P_o([Ca^{2+}]) \leq 1-p_{inh}(N^o)=(1-a)\exp(-(N^o-1)b)$. Therefore, 1-a is an upper bound for P_o at the cytosolic $[Ca^{2+}]$ that is reached when a single channel opens, while b^{-1} modulates the rate at which P_o decreases with cytosolic $[Ca^{2+}]$ (actually, with N^o). The parameters obtained with the fitting, a=0.8, b=1.8, imply that the upper bound, $(1-p_{inh})$, decreases from 0.2 (for $N^o=1$) at a cytosolic concentration, $[Ca^{2+}] \approx 40\mu M$, to 0.001 ($N^o=4$) at $[Ca^{2+}]$ between 120 and 160μM. These upper bounds are compatible with the observations of (3) at $[IP_3]=2\mu M$ and of (5) at $[IP_3]=33nM$. It is impossible to know the $[IP_3]$ during the experiments in which IP_3 is photo-released, therefore it is hard to validate or reject the model based on the determined behavior of p_{inh} (N^o). On the other hand, single IP_3R observations seem to be contradictory. However, we have suggested in (20) that one way to reconcile the observations of (3) and (5) is to assume that single IP_3R open proabibility is modulated by luminal Ca^{2+}. If the local $[Ca^{2+}]$ on the luminal side does not vary much during the time course of each experiment (which is one of the assumptions of our model, given the small amplitude of the puffs that we analyze), our simple model could then be used to assess the effect of luminal Ca^{2+} on single IP_3R. Similar conclusions can be obtained using the values of b and a determined for N=16.

We have also determined how the observed inter-puff time distributions and mean number of open channels during a puff would change if some of the parameters of our model were changed. The greatest difficulty in trying to test these predictions experimentally is the ability to introduce the necessary changes in a very controlled way so that the main assumptions of the model are not violated (if they are, we cannot guarantee that the conclusions still hold). In

particular, we have analyzed what could happen if the number of IP_3R's with IP_3 bound increased. Increasing this number could be achieved by increasing the light intensity with which IP_3 is uncaged during the experiment. That would serve as long as waves are not induced or the average Ca^{2+} level in between puffs does not increase too much compared with its basal value. We obtained that, in the model, the mean inter-puff time, $<\tau>$, decreased and the mean number of open channels during a puff, $<N^o>$, increased with N. Based on these results we concluded that $<\tau>$ should increase with the mean puff amplitude $<A>$ and this would occur both due to a larger amount of IP_3 or to a larger mean cluster size. In fact, we obtained some encouraging results by computing the mean puff amplitude and inter-puff time for the set of large clusters, for which we obtained a larger $<A>$ and a smaller $<\tau>$ than for the set of small clusters, although the differences were not statistically significant.

The fact that $1/\lambda_1>1/\lambda_2$ (a relation that we obtain from the fitting), means that, typically, each IP_3R becomes uninhibited faster than the rate at which it is challenged by basal Ca^{2+} to become open. We then used the model to investigate what its predictions were if we changed this inequality, namely, if λ_1 was increased leaving the other parameters fixed. We obtained that the mean inter-puff time decreased while the mean number of open channels during a puff decreased. The first observation is easy to understand: inter-puff frequency increases with λ_1 because IP_3R 's are challenged more often to become open. The other observation is due to the competition between channel challenging by basal Ca^{2+} (characterized by λ_1) and channel inhibition (characterized by λ_2). Namely, as $1/\lambda_1$ becomes comparable with $1/\lambda_2$, the limiting process for the occurrence of a puff becomes inhibition rather than channel opening. Therefore, if $1/\lambda_1$ is too small, the opening of the first channel in a cluster cannot induce the opening of many others because most of them are still inhibited. In this way, events tend to be smaller in size than when λ_1 is smaller. Testing this prediction experimentally is not so easy, because it is hard to alter λ_1 individually. In principle, it could be done by changing the basal Ca^{2+} level, however, it cannot be done by increasing this level by large amounts. Namely, for the assumptions of the model to still hold we need Ca^{2+} binding to the activating sites to be the limiting process for channel opening when channels are not inhibited (something that would be violated if the rates of Ca^{2+} and IP_3 binding become comparable) and we need Ca^{2+} -induced inhibition to be very rare at basal Ca^{2+} levels. Decreasing the basal $[Ca^{2+}]$, on the other hand, would not affect our assumptions. Therefore, one possibility would be the use of a slow buffer, like EGTA, that would not affect the values of $[Ca^{2+}]$ that could be attained around the channel's mouth during the opening of a single IP_3R, but that could alter the basal $[Ca^{2+}]$ level between puffs (varying λ_1). In fact, the use of moderate amounts of EGTA induces "event potentiation", *i.e.*an increment of puff amplitude, as reported in (25). It is not clear that this observed potentiation is related to a more likely release of inhibition in between puffs due to a lower amount of basal Ca^{2+} determined by the presence of EGTA, mainly because the experimental observation corresponds to events that occur almost simultaneously at many sites. The use of EGTA, on the other hand, "balkanizes" Ca^{2+} signals (17), which can be related to the decrease of λ_1 that could result from a lower cytosolic $[Ca^{2+}]$ between puffs. Therefore, these two observations seem to fit within the dual role that we envisage for cytosolic Ca^{2+} in our model. The use of relativaly large amounts of BAPTA in the experiments of (25), on the other hand, induce an almost permanent Ca^{2+} release from internal stores, where individual puffs cannot be distinguished. In principle, very large amounts of BAPTA could alter the distribution of cytosolic Ca^{2+} within the cluster, even when a single IP_3R is open. Therefore, the presence of BAPTA could not only change "λ_1", but also decrease p_{inh} (N^o) for each value of the number of open channels, N^o. Our model cannot describe a situation in which cytosolic Ca^{2+} does not go back

to its basal value almost immediately after the occurrence of a puff. However, the fact that by decreasing p_{inh}, the mean inter-puff time decreases is in accordance with the observation of an almost permanent release of Ca^{2+} in the presence of large amounts of BAPTA. The effect of assuming that single IP_3R inhibition by cytosolic Ca^{2+} is moderated (due to the presence of a fast buffer like BAPTA) should be similar to the effect of assuming that more channels with IP_3 bound are present in the cluster. In fact, we observe that, according to the model, both the mean inter-puff frequency and the mean number of open channels during a puff increase with increasing N. Although not completely conclusive, an analysis of the subset of clusters that displayed the largest puff amplitudes indicates that this is indeed the case.

Even though simple, our model allows the extraction of single IP_3R information from the analysis of experiments in which several IP_3R 's work concordantly to generate a puff. In this respect, the existence of an inhibited state with mean time duration of the order of a few seconds is a feature that could be contrasted against mean closed times of single IP_3R 's, as we did before. Different values of mean closed times have been reported in the literature for the same amount of IP_3, which we have interpreted in (20) as due to the use of diverse amounts of luminal Ca^{2+} in the various experiments. Mean closed times are also dependent on $[IP_3]$, which is a variable that is hard to know in optical experiments. If the assumption that luminal Ca^{2+} remains approximately constant during the time course of the experiments that we analyze is correct, then we can determine with which values of $[IP_3]$ and luminal $[Ca^{2+}]$ the parameters of our model are compatible. Thus, our model can help us build a comprehensive picture of single IP_3R dynamics. However, IP_3R inhibition due to cytosolic Ca^{2+} is not the only possible explanation behind the inter-puff time and puff amplitude dependence that we report in this paper. Namely, the fact that smaller puff amplitudes are observed if not enough time has elapsed from the previous one could also be due to a local depletion of luminal Ca^{2+} that would result in a smaller single channel current. A change in luminal Ca^{2+} could also affect the open probability of the IP_3R 's. In the case of sparks in myocytes, in which Ca^{2+} release from internal stores occurs through ryanodine receptors, most experimental evidence points to the role of luminal Ca^{2+} as a modulator of single receptor's open probability as the basic effect that signals spark termination and that determines the refractory time (12,13). Right now, we cannot rule out that a similar control is taking place in oocyte's puffs too. Comparing the values of λ_1 and λ_2 obtained with our model with the values that can be determined from single IP_3R experiments could also be used to validate or reject the hypothesis that cytosolic Ca^{2+} is the only responsible for the inter-puff time puff amplitude dependence reported in this paper. At this stage, more experiments and analyses are necessary to arrive at a definite conclusion. In particular, experiments in which luminal Ca^{2+} dynamics is altered (*e.g.*, via the inclusion of certain buffers) would help us assess the role of luminal Ca^{2+} on our observations. In any case, we think that our approach sheds light on the unveiling of the elusive behavior of IP_3R 's in their native environment.

Acknowledgments
This research is supported by Universidad de Buenos Aires, PICT 03-08133 of ANPCyT (Argentina), and N.I.H. grant 1R01GM65830-01. S.P.D. is a member of the Carrera del Investigador Científico (CONICET).

1. M. Iino, 1990. Biphasic calcium dependence of inositol trisphosphate induced calcium release in smooth muscle cells of the guinea pig Taenia caeci. J. Gen. Physiol. 95:1103-1122

2. E.A. Finch, T.J. Turner, et al, 1991. Calcium as a co-agonist of inositol 1,4,5-trisphosphate-induced calcium release, Science 252:443-446
3. I. Bezprozvanny, J. Watras, and B.E. Ehrlich, 1991. Bell-shaped calcium-response of Ins(1,4,5)P3- and calcium-gated channels from endoplasmic reticulum of cerebellum. Nature 351:751-754
4. J. Ramos-Franco, M. Fill, and G.A. Mignery, 1998. Isoform-Specific Function of Single Inositol 1,4,5-Trisphosphate Receptor Channels. Biophysical Journal 75:834-839
5. D.O. Mak, S. McBride and J.K. Foskett, 1998. Inositol 1,4,5-trisphosphate activation of inositol tris-phosphate receptor Ca2+ channel by ligand tuning of Ca2+ inhibition. Proc. Natl. Acad. Sci. (USA) 269:7238-7242
6. Y. Yao, J. Choi., I. Parker. 1995. Quantal puffs of intracellular Ca2+ evoked by inositol trisphosphate in Xenopus oocytes. J. Physiol. 482:533-553.
7. X. Sun, N. Callamaras, J.S. Marchant, I. Parker. 1998. A continuum of InsP3 -mediated elementary Ca2+ signalling events in Xenopus oocytes. J. Physiol. 509:67-80.
8. D. Thomas, P. Lipp, S.C. Tovey, M.J. Berridge,W. Li,R.Y. Tsien, and M.D. Bootman , 2000. Microscopic properties of elementary Ca2+ release sites in non-excitable cells. Curr Biol. 10(1): 8-15.
9. N. Melamed-Book, S.G. Kachalsky, I. Kaiserman, and R. Rahamimoff, 1999. Neuronal calcium sparks and intracellular calcium “noise”. Neurobiology 96:15217-15221
10. S. Koizumi, M.D. Bootman, L.K. Bobanovic, M.J. Schell, M.J. Berridge, and P. Lipp, 1999. Characterisation of elementary Ca2+ release signals in NGF-differentiated PC12 cells and hippocampal neurones. Neuron 22:125-137.
11. J. Huser and L.A. Blatter, 1997. Elementary events of agonist-induced Ca2+ release in vascular endothelial cells. Am J Physiol. 42:C1775-1782.
12. D. Terentyev, S. Viatchenko-Karpinski, H. H. Valdivia, A. L. Escobar and S. Gyorke, 2002. Luminal Ca2+ Controls Termination and Refractory Behavior of Ca2+-Induced Ca2+ Release in Cardiac Myocytes. Circ. Res. 91: 414-420.
13 . P. Szentesi, C. Pignier, M. Egger, E. G. Kranias and E. Niggli, 2004. Sarcoplasmic Reticulum Ca2+ Refilling Controls Recovery From Ca2+-Induced Ca2+ Release Refractoriness in Heart Muscle. Circ. Res. 95:807-813.
14. T. Nguyen, W-C Chin and P. Verdugo, 1998. Role of Ca2+/K+ ion exchange in intracellular storage and release of Ca2+. Nature 395:908-912.
15. I. Parker, N. Callamaras, W.G. Wier, 1997. A high–resolution, confocal laser scanning microscope and flash photolysis system for physiological suties. Cell Calcium 2:441-452
16. A.C. Ventura, L. Bruno, A. Demuro, I. Parker and S.P. Dawson, 2005. A model-independent algorithm to derive Ca2+ fluxes underlying local cytosolic Ca2+ transients. Biophys. J. 88:2403-2421.
17. N. Callamaras and I. Parker, 2000. Phasic characteristic of elementary Ca^{2+} release sites underlies quantal responses to IP_3. EMBO J. 19:3608-3617.
18. W.J.Conover, Practical nonparametric statistics.Wiley, pp. 558
19. R. Thul and M. Falcke, 2004. Release Currents of IP3 Receptor Channel Clusters and Concentration Profiles. Biophys. J. , 86:2660-2673.
20. D. Fraiman and S. Ponce Dawson, 2004. A model of the IP3 receptor with a luminal calcium binding site: stochastic simulations and analysis. Cell Calcium 35:403-413.
21. J. Marchant and C. Taylor, 1998. Rapid activation and partial inactivation of inositol trisphosphate receptors by inositol trisphosphate. Biochemistry 33:11524-11533.
22. J. Shuai and I. Parker, 2005. Optical single-channel recording by imaging Ca2+ flux through individual ion channels: theoretical considerations and limits to resolution. Cell Calcium 37:283-299.

23. C.E. Adkins and C.W. Taylor,1999. Lateral inhibition of inositol 1,4,5-trisphospate receptors by cytosolic Ca2+. Curr. Biol. 9:1115-1118.
24. L. Bruno, private communication
25. S. Dargan and I. Parker, 2004. Buffer kinetics shape the spatiotemporal patterns of IP3-evoked Ca2+ signals. J. Physiol 553:775-788
26. G. Solovey, D. Fraiman, B. Pando and S. Ponce Dawson, 2005 (to be published).
27. S. Swillens, G. Dupont, L. Combettes and P. Champell, 1999. From calcium blips to calcium puffs: Theoretical analysis of the requirements for interchannel communication. Proc. Natl. Acad. Sci (USA) 96:13750-13755.
28. G.W. De Young and J. Keizer, 1992. A single-pool inositol 1,4,5-trisphosphate-receptor agonist-stimulated-based model for oscillations in Ca2+ concentration. Proc. Natl. Acad. Sci.(USA) 89:9895-9899
29. N. Callamaras and I. Parker, 1999. Initiation of IP_3-mediated Ca2+ waves in Xenopus Laevis oocytes. EMBO J., 18:5285-5299
30. D.O. Mak, S. McBride and J.K. Foskett, 2001. ATP-dependent Adenophostin Activation of Inositol 1,4,5-Trisphosphate Receptor Channel Gating. J. Gen. Physiol. 117:299-314
31. I. Bezprozvanny and B.E. Ehrlich, 1994. Inositol (1,4,5)-trisphosphate (InsP3)-gated Ca Channels from Cerebellum: Conduction Properties for Divalent Cations and Regulation by Intraluminal Calcium. J. Gen. Physiol. 104:821-856

FIGURE LEGENDS

Fig 1. **A**) Linescan image illustrating puffs evoked by sustained photorelease of IP_3. The y axis represents distance along the scan line, and time runs from left to right. Increases in fluorescence ratio ($\Delta F(x,t)/F_0$) are depicted on a pseudocolor scale, with 'warmer' colors corresponding to increasing ratio (increasing free [Ca^{2+}]). The UV photolysis light was turned on about 10 s before the beginning of the record. **B**) Traces show fluorescence profiles monitored from 5 of the puff sites in (A). Arrowed line illustrates the measurement of elapsed time τ between two successive puffs.

Fig. 2. Maximum puff amplitude at each site.

Fig. 3. Histograms of puff amplitude, *A* (A) and inter-puff time, τ (B).

Fig. 4. Puff amplitude (A_n) histogram conditional to: (A) τ_{n-1} <1.4s ; (B) τ_{n-1} >3.27s. The differences in the distribution functions are statistically significant (p-values<0.001).

Fig. 5. Inter-puff time (τ_n) histogram conditional to: (A) A_n <0.092 ; (B) A_n >0.134 . The differences in the distribution functions are statistically significant (p-values<0.04).

Fig. 6. (A) Conditional amplitude distribution function for the sets of small previous inter-puff times, τ_{n-1}, containing the 17% (curve 1) and the 50% smallest values (curve 2) of τ_{n-1} and for the set of large previous inter-puff times containing the 17% (curve 4) and the 50% largest values (curve 3) of τ_{n-1}. In both cases the differences in the distribution functions are statistically significant (p-values<0.002). (B) Similar to (A) but for the inter-puff time distribution function conditional to small or large values of the previous puff amplitude, A_n. The various curves correspond to the sets containing the 17% smallest (curve 1), the 50% smallest (curve 2), the 17% largest (curve 4) and the 50% largest (curve 3) values of A_n. The Kolmogorov test gives p-value=0.04 comparing curves 1 and 3, and 0.18 for 2 and 4.

Fig. 7. A simple model of cluster dynamics in terms of individual channels. Random binding events of Ca^{2+} ions to activating sites on IP_3R are marked by crosses. If the channel is inhibited (depicted with dashed lines), nothing happens. If the channel is uninhibited (depicted with solid lines), it opens, resulting in opening of all other uninhibited channels in the cluster to generate a puff. During each puff, some of the uninhibited channels become inhibited, with a probability that is a (saturating) increasing function of the puff amplitude (characterized by the number of channels that opened during the puff, N^o). At any time, an inhibited channel may spontaneously become uninhibited (indicated with a solid black circle) with a probability per unit time, λ_2. The schematic illustrates a cluster of 5 channels, which generates 3 puffs involving varying numbers of open channels.

Fig. 8. Histogram of number of open channels during a puff (A) and of inter-puff times (B) obtained from stochastic simulations of our model using $N=4$, $\lambda_1=0.225s^{-1}$, $\lambda_2=0.4s^{-1}$ $a=0.8$ and $b=1.8$.

Fig. 9. Histograms of open channels, N^o conditional to "small", τ_{n-1} <1.4s , (A) and "large", τ_{n-1} >3.27s, (B) previous inter-puff times.

Fig. 10. Conditional distributions of inter-puff times, τ for the set of small, $N^o \leq 2$ (A) and large, $N^o \geq 3$ (B) previous number of open channels.

Fig. 11. (A) Mean number of open channels during a puff, $<N^o>$ (crosses) and mean inter-puff time, $<\tau>$ (asterisks) as a function of the number of functional channels in the cluster, *N*. (B) Mean number of open channels during a puff, $<N^o>$ (crosses) and mean inter-puff time, $<\tau>$ (asterisks) as a function of the rate of Ca^{2+} binding to a channel in the cluster, λ_1.

Fig. 12. Mean inter-puff time, $<\tau>$, as a function of the mean number of open channels during a puff, $<N^o>$ for N=2, 3, 4, 5, 6, 7, and 8 (A) and for various values of λ_1 (B).

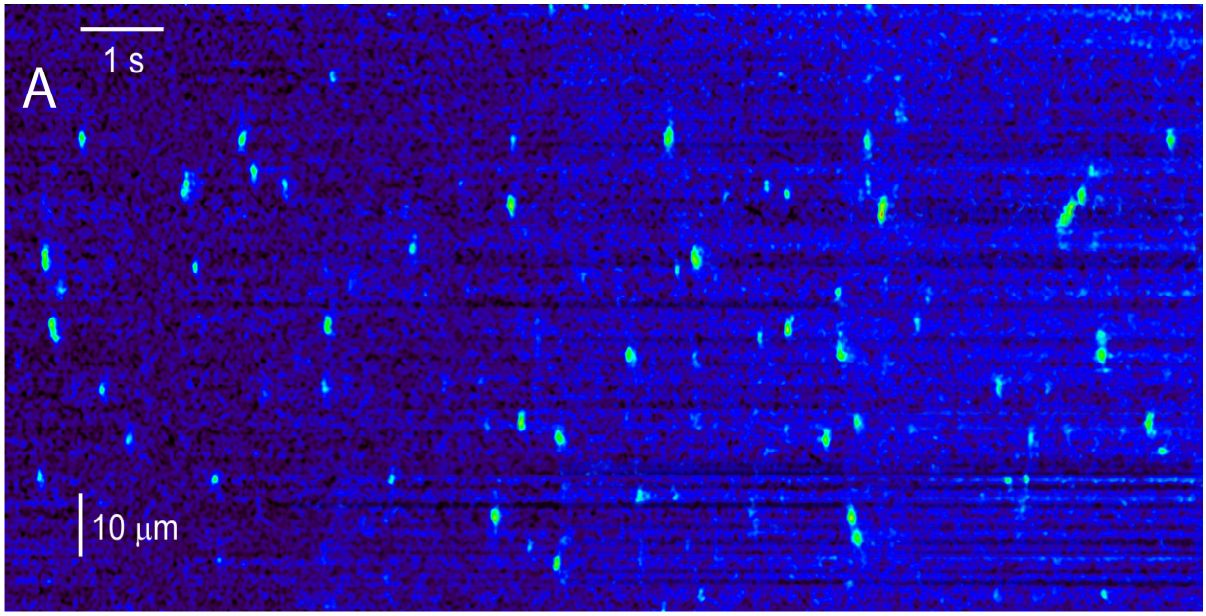

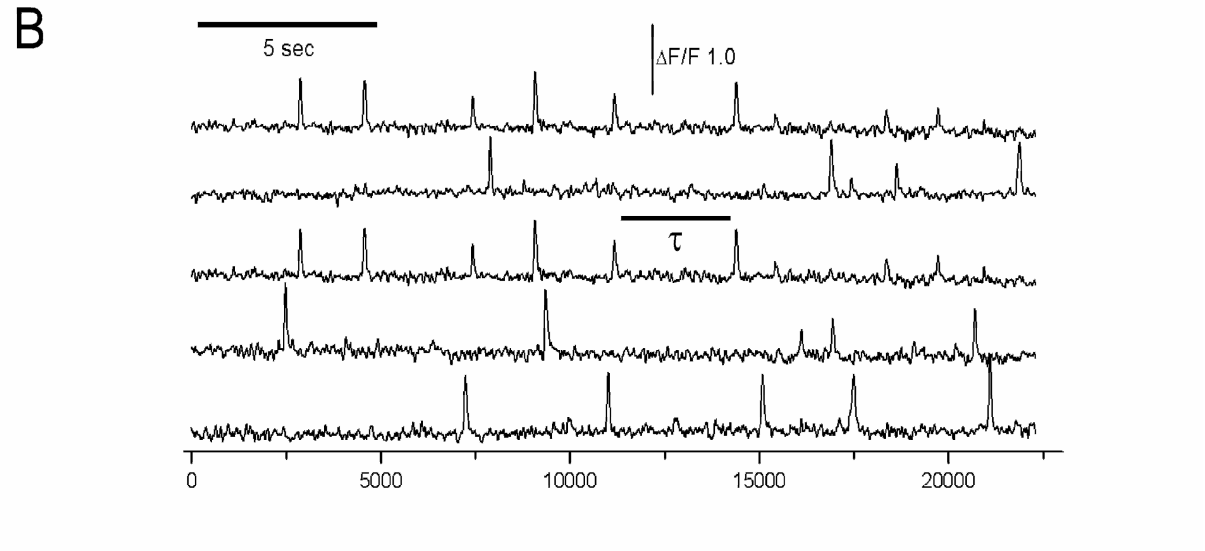

Fig 1

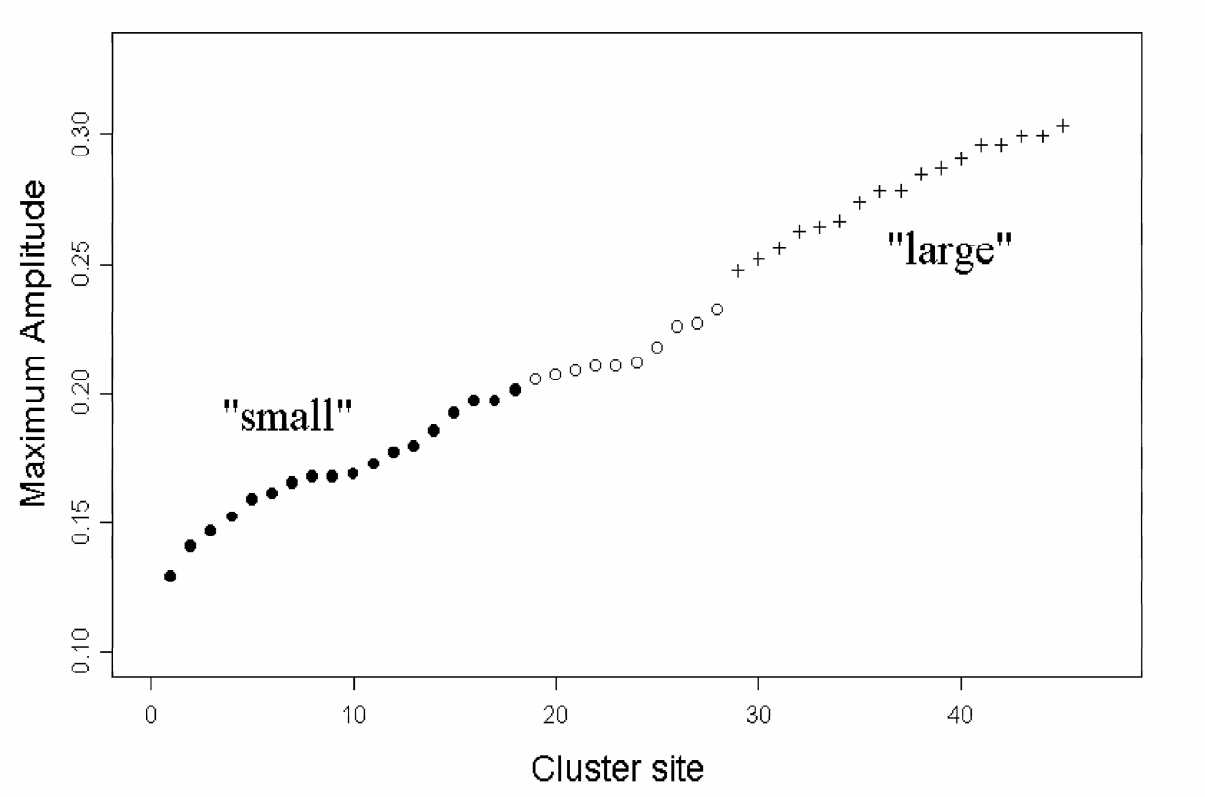

Fig. 2

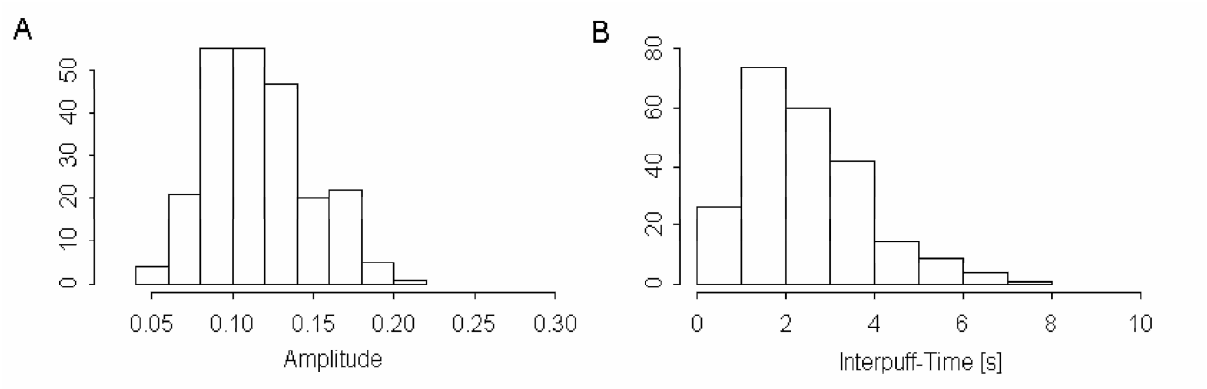

Fig. 3

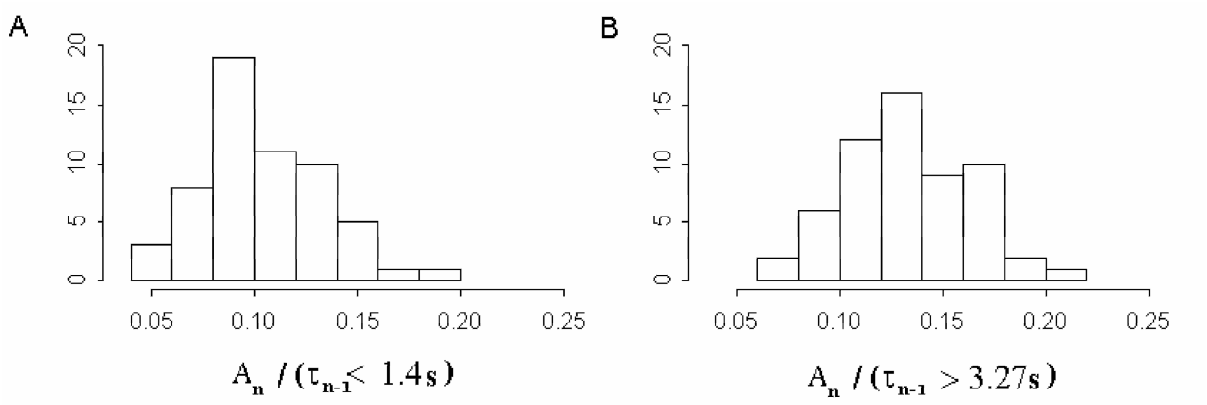

Fig. 4

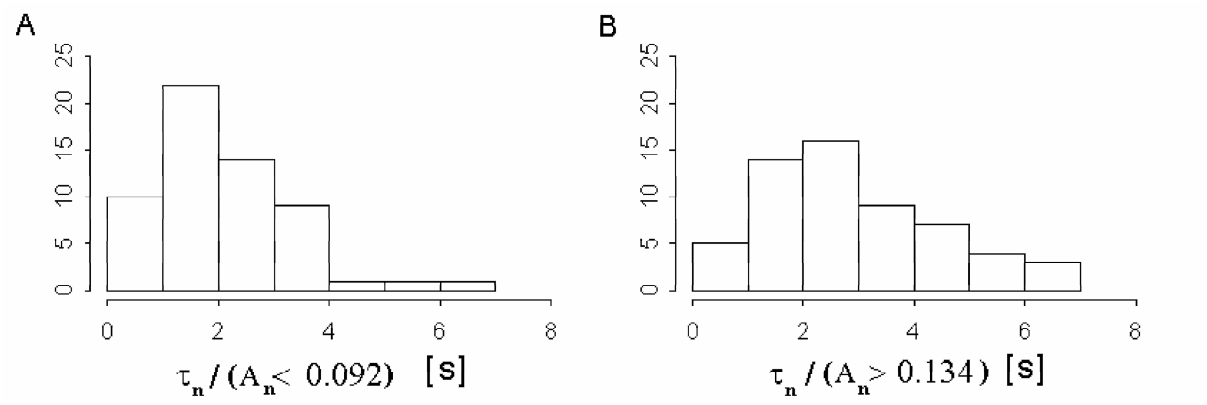

Fig. 5

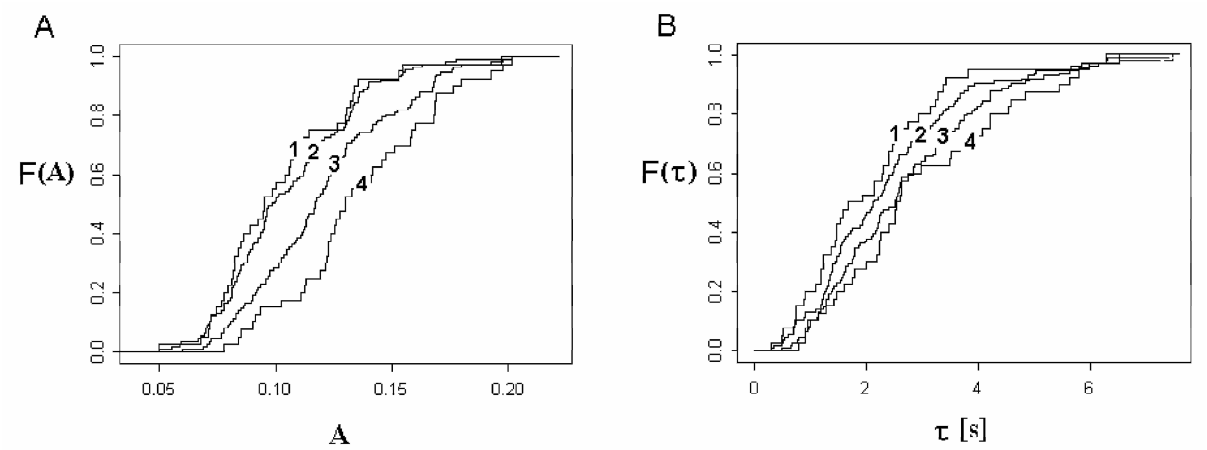

Fig. 6

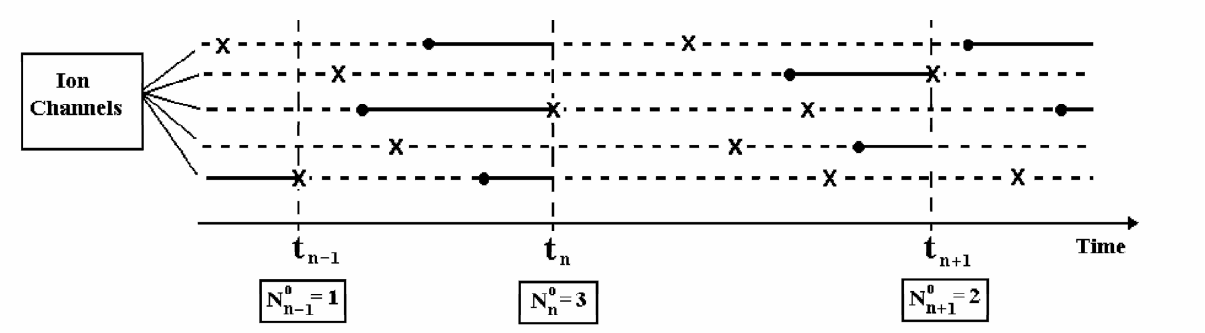

Fig. 7

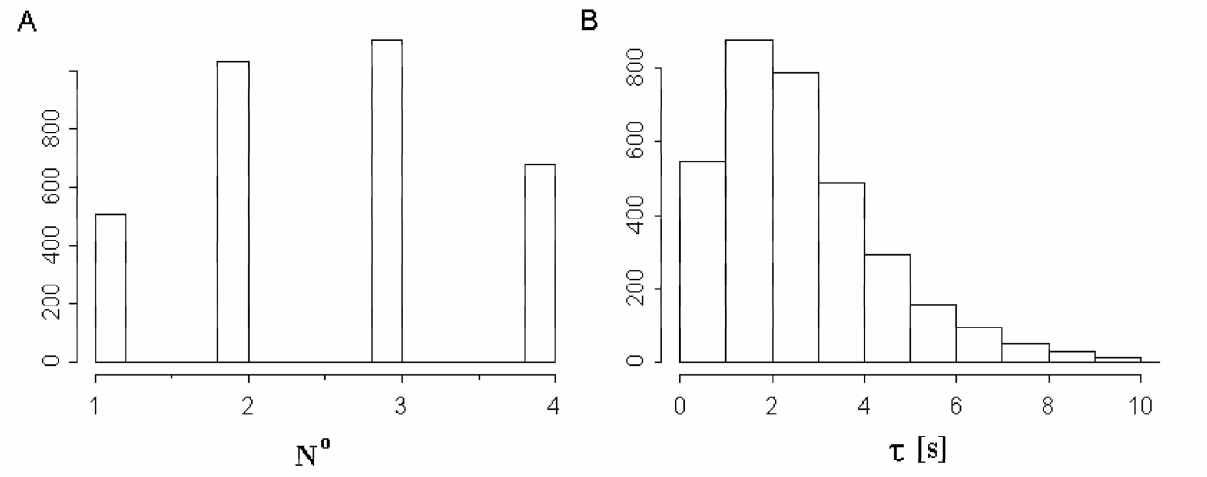

Fig. 8

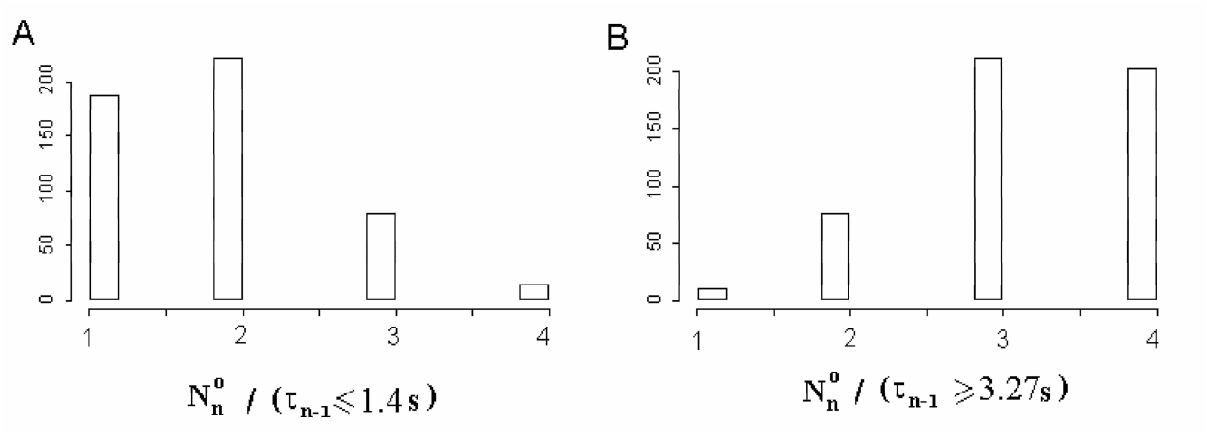

Fig. 9

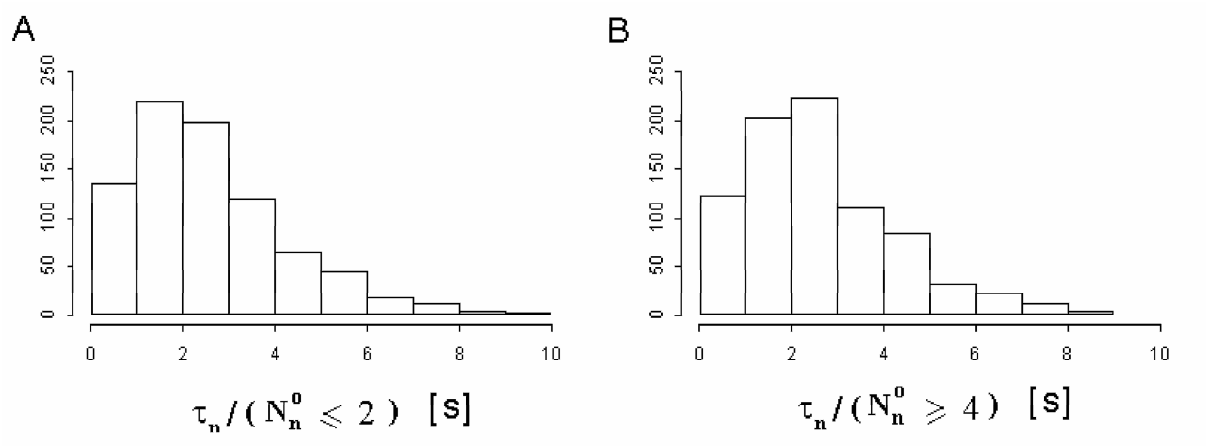

Fig. 10

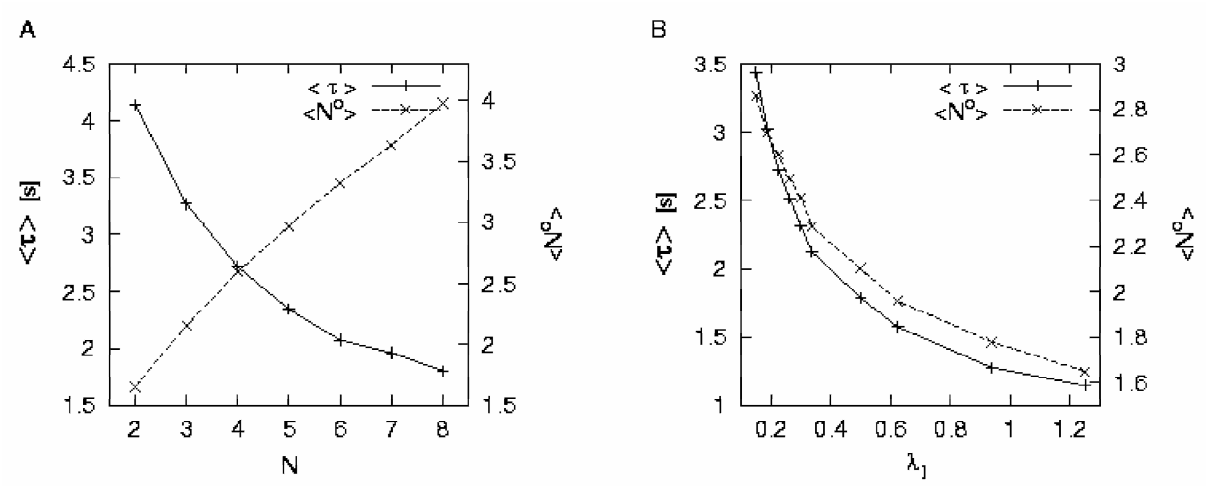

Fig. 11

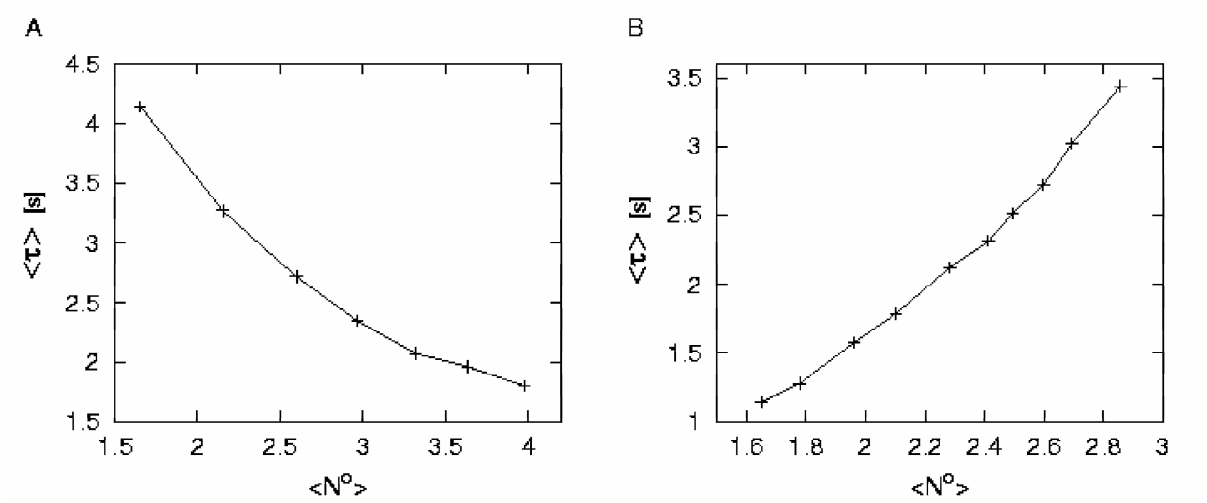

Fig. 12